Kolmogorov Turbulence Coexists with Pseudo-Turbulence in Buoyancy-Driven Bubbly Flows

Vikash Pandey [1,2,*] Dhrubaditya Mitra [2] and Prasad Perlekar [1,†]

[1] *Tata Institute of Fundamental Research, Gopanpally, Hyderabad 500046, India*
[2] *Nordita, KTH Royal Institute of Technology and Stockholm University, Hannes Alfvéns väg 12, 10691 Stockholm, Sweden*

We investigate the spectral properties of buoyancy-driven bubbly flows. Using high-resolution numerical simulations and phenomenology of homogeneous turbulence, we identify the relevant energy transfer mechanisms. We find (a) at a high enough Galilei number (ratio of the buoyancy to viscous forces) the velocity power spectrum shows the Kolmogorov scaling with a power-law exponent $-5/3$ for the range of scales between the bubble diameter and the dissipation scale (η). (b) For scales smaller than η, the physics of pseudo-turbulence is recovered.

The flow behind an array of cylinders or a grid, either moving or stationary, provides an ideal testbed to verify and scrutinize the statistical theories of turbulence [1]. What is the flow generated when a fluid is stirred by a dilute suspension of bubbles as they rise due to buoyancy? This question has intrigued researchers for the past three decades due to their occurrence in both industrial and natural processes [2–7]. Experiments [8–13] and numerical simulations [14–16] show that flows generated by dilute bubble suspensions are chaotic and originate due to the interplay of viscous, inertial, and surface tension forces. The complex spatiotemporal flow is called "pseudo-turbulence" or "bubble induced agitation" [3,5].

As is typical for chaotic flows, pseudo-turbulence is characterized by the power spectrum of its velocity fluctuations $E(k)$, which shows a power law scaling $E(k) \sim k^{-\alpha}$ with an exponent $\alpha \gtrsim 3$ in the wave number range $k \gtrsim k_d$, where $k_d = 2\pi/d$ and d is the bubble diameter [8,12]. Lance and Bataille [8] argued that the balance of energy production with viscous dissipation may explain the observed scaling. Recent numerical studies conducted for experimentally accessible Galilei numbers Ga (the ratio of buoyancy to viscous dissipation), show that the net production has contributions both from the advective nonlinearity and the surface tension [11,14–16].

In homogeneous and isotropic turbulence (HIT) the energy injected at an integral scale $\mathcal{L}$ is transferred to dissipation scale $\eta \ll \mathcal{L}$, via the advective interactions without dissipation while maintaining a constant energy flux. This intermediate range of scales between η and $\mathcal{L}$ is called the inertial range. At scale smaller than η the advective interactions balance viscous dissipation [17]. Clearly within the phenomenology of homogeneous and isotropic turbulence, pseudo-turbulence is a dissipation range phenomena with the additional complexity due to

surface tension forces. Is it possible to have an inertial range in buoyancy driven bubbly flows?

In this Letter, we present state-of-the-art direct numerical simulations of buoyancy driven bubbly flows, at high resolution, which allows us to access Ga > 1000 which has never been achieved before in either experiments or numerical simulations. Our multiphase simulations model a dilute suspension of "gas" bubbles of lighter phase (density ρ_1) dispersed in the heavier "liquid" phase (density ρ_2). The density contrast is parametrized by the Atwood number, At $\equiv (\rho_2 - \rho_1)/(\rho_2 + \rho_1)$. We consider both small (0.04) and large (0.8,0.98) values for At. We use two different codes for these two cases. In both of these cases, we find, for the first time, a direct evidence for Kolmogorov scaling, $E(k) \sim k^{-5/3}$, for $k_d \leq k \lesssim 1/\eta$. For scales smaller than η, the physics of pseudo-turbulence is recovered. By analyzing the scale-by-scale energy budget we uncover the mechanism by which the Kolmogorov scaling emerges: for high enough Ga, for both small and larger At, there is an intermediate range of scales over which the contribution from advection dominates over all other contributions (including surface tension) in the kinetic energy budget. This is the range over which Kolmogorov scaling is observed.

We study the dynamics of bubbly flow using multiphase Navier-Stokes equations [14] for an incompressible velocity field $\boldsymbol{u} = (u^x, u^y, u^z)$,

$$\rho(\partial_t \boldsymbol{u} + \boldsymbol{u} \cdot \nabla \boldsymbol{u}) = \mu \nabla^2 \boldsymbol{u} - \nabla p + \boldsymbol{F}^\sigma + \boldsymbol{F}^g, \quad \text{where} \quad (1a)$$

$$\boldsymbol{F}^g \equiv [\rho(c) - \rho_a]\boldsymbol{g} = \text{At}(\rho_2 + \rho_1)(c - c_a)\boldsymbol{g}, \quad \text{and} \quad (1b)$$

$$\boldsymbol{F}^\sigma \equiv \int \sigma\kappa\hat{\boldsymbol{n}}\delta(\boldsymbol{x} - \boldsymbol{x}_b)ds, \quad (1c)$$

TABLE I. Parameters of simulations. The Bond number Bo $= 1.75$, number of bubbles $N_b = 12$, the diameter of the bubble $d = 1.08$, $L = 2\pi$, $\rho_2 = 1.0$, and the volume fraction of the bubbles $\phi = 3.2\%$ are same in all the runs. For all the runs $\mathcal{L} \sim d$, and the statistics are averaged over a period of at least $5\tau_L$ in the stationary state (see Supplemental Material [27]). Total energy injection rate $\epsilon^g = 0.031 \pm 0.002$ in all the cases.

runs	R1	R2	R3	R4	R5	R6	vof-R5	R7	R8	R9
N	256	512	512	512	720	720	1024	288	504	504
Ga	103	302	403	605	1029	2057	1029	340	1059	1489
At	0.04	0.04	0.04	0.04	0.04	0.04	0.04	0.8	0.8	0.98
Re_λ	11.8	30.7	37.9	47.8	60.7	96.9	60.7	28.8	69.3	88.1
$\mathcal{L}/\eta$	12.6	26.3	29.5	38.8	50.4	80	50.4	20.5	46	56.0

where the bulk viscosity μ is assumed to be identical in both the phases, and p is the pressure. An indicator function c, distinguishes the liquid ($c = 1$) and the gas ($c = 0$) phase [18,19]. The density field $\rho(c) = \rho_2 c + \rho_1(1 - c)$. In Eq. (1), the buoyancy force is F^g, $c_a \equiv (1/V) \int c\, dV$ is the indicator function averaged over the volume V of the simulation domain, $\rho_a = \rho_1 + (\rho_2 - \rho_1)c_a$ is the average density, $g \equiv -g\hat{z}$ is the acceleration due to gravity, and $\hat{z}$ is the unit vector along the vertical (positive z) direction. The surface tension force is denoted by F^σ, where σ is the coefficient of the surface tension, κ is the local curvature of the bubble-front located at x_b, $\hat{n}$ is the unit normal, and ds is the infinitesimal surface area of the bubble.

For the small At $= 0.04$ case, we invoke Boussinesq approximation [20] wherein the density variations can be ignored $\rho \approx \rho_a$, and the buoyancy force simplifies to $F^g = 2\rho_a At(c - c_a)$ [14,15]. We solve Eq. (1) numerically using the pseudo-spectral method [21] in a three-dimensional periodic domain where each side is of length L, discretized uniformly into N collocation points. We numerically integrate the bubble phase using a front-tracking method [14,19,22]. For time evolution, we use a second-order exponential time differencing scheme [23] for Eq. (1) and a second-order Runge-Kutta scheme to update the front. For the large At $= 0.8$, and 0.98, we use the front tracking module of an open-source multiphase solver PARIS [24], where both spatial and temporal derivatives are approximated using a second-order central-difference scheme.

Consistent with the experiments designed to study buoyancy driven bubbly flows [8,12,13] we choose the

volume fraction of the bubbles $\phi \leq 5\%$. At these volume fraction, the effects coalescence or breakup of the bubbles can be ignored [25]. The front-tracking scheme is ideally suited to study this parameter range because it ignores both coalescence and breakup. For one representative case we also perform volume-of-fluid (VOF) simulation (vof-R5) using PARIS—VOF simulations allow coagulation and breakup—to confirm that coalescence plays no significant role.

In what follows, the following nondimensional numbers will be used: Atwood number At defined previously, the Galilei number, $\mathrm{Ga} \equiv \sqrt{(\rho_2 - \rho_1)gd^3/\rho_2\nu^2}$, the Bond number $\mathrm{Bo} \equiv (\rho_2 - \rho_1)gd^2/\sigma$, the integral scale Reynolds number $Re_{\mathcal{L}}^{3/4} \equiv \mathcal{L}/\eta$, the Taylor-microscale Reynolds number $Re_\lambda \equiv u_{rms}^2\sqrt{15\rho_2/(\nu\epsilon^g)}$. Here we have used kinematic viscosity $\nu = \mu/\rho_2$, the large eddy turnover time $\tau_L \equiv \mathcal{L}/u_{rms}$, the root-mean-square velocity, u_{rms}, the energy injection rate by the buoyant forces [26], $\epsilon^g \equiv (1/V) \int F^g \cdot u\, dV$, integral length scale $\mathcal{L} \equiv (3\pi/4)[\sum_k E(k)/k]/\sum_k E(k)$, and the Kolmogorov dissipation scale $\eta \equiv (\rho_a\nu^3/\epsilon^g)^{1/4}$ The different parameters of our simulations are given in Table I.

We start our simulation by placing N_b bubbles randomly in the domain. It takes around $4.5\tau_L$ for our simulation attain a statistically stationary state. Once it is reached, all our data are averaged over at least $5\tau_L$. In Fig. 1 we show the isocontour plot of the z component of vorticity $\omega^z = (\nabla \times u) \cdot \hat{z}$. As the Ga ($Re_\lambda$) is increased, not only the intense vortical regions in the field increases, we observe flow structures at much smaller scales as well.
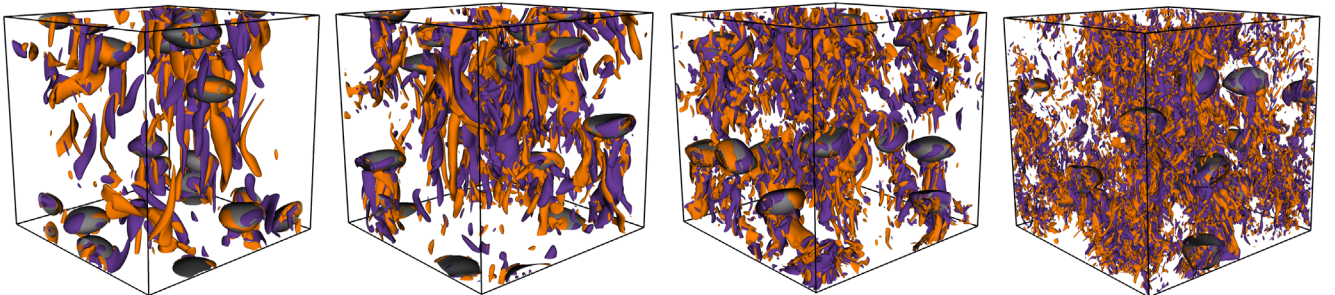

FIG. 1. The isocontour plot of the z component of the vorticity $\omega^z = (\nabla \times u) \cdot \hat{z}$ for (left to right) Ga $= 302, 605, 1029$, and 2057. We show the contour corresponding to $\pm\langle(\omega^z)^2\rangle^{1/2}$ in purple and orange, respectively. The bubbles are represented using gray contours.

Next we investigate the power spectrum of velocity fluctuations:

$$E(k) = \frac{1}{2}\sum_{\boldsymbol{k}}\langle\hat{\boldsymbol{u}}(\boldsymbol{k})\hat{\boldsymbol{u}}(-\boldsymbol{k})\rangle\delta(|\boldsymbol{k}| - k), \qquad (2)$$

where $\hat{\boldsymbol{u}}(\boldsymbol{k})$ is the Fourier transform of the velocity field $\boldsymbol{u}$, $\boldsymbol{k}$ the wave vector, and $\langle\cdot\rangle$ denotes the spatiotemporal average over the statistically stationary state of turbulence. Kolmogorov theory of turbulence shows that, in homogeneous and isotropic turbulence, $E(k)$ for different Reynolds numbers collapses onto a single curve if we use η as the characteristic length scale and $E_0 = (\epsilon^g\nu^5/\rho_2)^{1/4}$ as the characteristic energy scale, which we use henceforth. In Fig. 2(a) we show that, even for buoyancy driven bubbly turbulence, the same data collapse holds for scales $k \gtrsim k_d$. For small Ga number we obtain the pseudo–turbulence regime [8,12–14] for $k \gtrsim 0.3/\eta$. As the Ga increases a scaling range with an exponent of approximately $-5/3$ emerges for $k_d \lesssim k \lesssim 0.3/\eta$. This is a novel, previously unobserved scaling in bubbly flows. The scaling range increases with Ga; it is almost nonexistent for Ga $= 100$ and extends up to almost half a decade for Ga $= 2057$. The $-5/3$ scaling range is best seen in Fig. 2(b) where we plot the
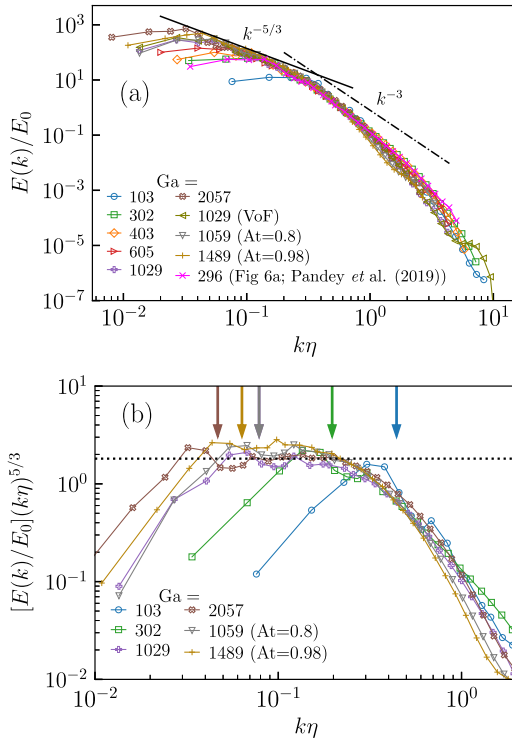

FIG. 2. (a) Log-log plot of the normalized velocity power spectra $E(k)$ as a function of $k\eta$ for various Ga. We observe Kolmogorov scaling $E(k) \sim k^{-5/3}$ for $k\eta \lesssim 0.3$, and the pseudo-turbulence scaling $E(k) \sim k^{-3}$ for $k\eta \gtrsim 0.3$. (b) The velocity power spectra for different Ga compensated by $k^{5/3}$. In (b) the vertical arrows show the wave number corresponding to the bubble diameter $k_d\eta$.

spectra compensated with $k^{5/3}$. As we have used η as our characteristic length scale the Fourier mode k_d, shown by an arrow, appears at different locations in this plot. As Ga is increased k_d moves to the left thereby the $-5/3$ scaling range emerges.

Note that due to rising bubbles, in principle, our flow is anisotropic. Here and henceforth, following the standard practice in bubbly turbulence [8,14,16], we use the isotropic spectra which is the projection of the general anisotropic spectra on to the isotropic sector [32]. In the Supplemental Material [27], which includes Ref. [32], we show that for our simulations the anisotropic contribution is negligible at all scales except k in the neighborhood of k_d.

We now describe how Kolmogorov scaling emerges at both small and large At by studying the scale-by-scale energy budget equation:

$$\partial_t\mathcal{E}_K = -\Pi_K - \mathcal{F}_K^\sigma + \mathcal{P}_K - \mathcal{D}_K + \mathcal{F}_K^g. \qquad (3)$$

Here $\mathcal{E}_K$ is the kinetic energy contained up-to wave number K. Here Π_K, $\mathcal{F}_K^\sigma$, $\mathcal{P}_K$, $\mathcal{D}_K$, and $\mathcal{F}_K^g$ are the contributions from the advective term, surface tension, pressure, viscous dissipation, and buoyancy from Eq. (1) [27].

The scale-by-scale budget for low At $= 0.04$.—We follow Refs. [17,28,29,33] to derive Eq. (3). We consider stationary state, hence $\partial_t\mathcal{E}_K = 0$ and we use Boussinesq approximation, hence $\mathcal{P}_K = 0$. We plot all the others terms of Eq. (3) as a function of K in the top row of Fig. 3 for large and small Ga. As expected [14], bubbles inject energy into the flow at scales comparable to the bubble diameter —$\mathcal{F}_K^g$ monotonically increases and saturates around $K \approx k_d$. From the perspective of the Kolmogorov theory of turbulence [17] the buoyancy injection term $\mathcal{F}_K^g$ is the large scale driving force active at scales around k_d. Following Ref. [17], consider a fixed $K \gg k_d$ and take the limit $\nu \to 0$ (Ga $\to \infty$). Then $\lim_{\nu\to0}\mathcal{D}_K \approx 0$, holds and the flux balance equation reads

$$\Pi_K + \mathcal{F}_K^\sigma = \epsilon^g. \qquad (4)$$

Because the injection is limited to Fourier modes around k_d, for $K \gg k_d$, $\mathcal{F}_K^g \approx \epsilon^g$ is a constant. In homogeneous and isotropic turbulence in absence of bubbles the dissipative effects become significant around 8 to 10η [34]. We find 3η is a reasonable approximation in our case. Thus, Eq. (4) is expected to be valid for $k_d < K \lesssim 0.3/\eta$—this range is shaded with light blue in Fig. 3. Within the shaded region $\Pi_K \gg \mathcal{F}_K^\sigma$, hence $\Pi_K \approx \epsilon^g/2$ is a constant leading to the Kolmogorov $-5/3$ scaling in the energy spectrum [17]. Even at Ga $= 2057$, the $-5/3$ scaling range is at best close to a decade. In Fig. 3(b), for Ga $= 302$ the shaded region has practically disappeared. For this and other runs with smaller Ga, we expect to observe pseudo-turbulence where none of the three fluxes, $\mathcal{F}_K^\sigma$, Π_K, and $\mathcal{D}_K$, can be ignored. A detailed discussion on the flux balance in the
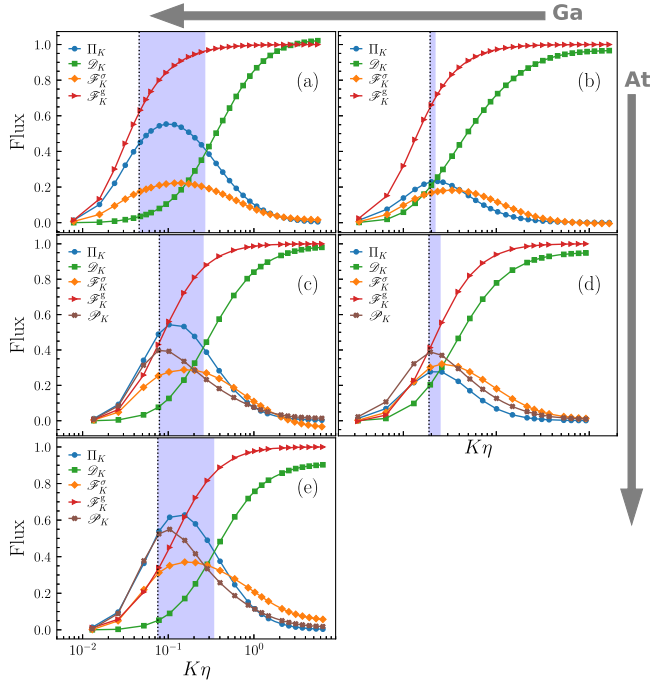
FIG. 3. Semi-log plot of the different terms in scale-by-scale budget for low Atwood number At = 0.04 (top row) with Ga = 2057 (a) and Ga = 302 (b); At = 0.8 (middle row) for Ga = 1029 (c), Ga = 345 (d); and At = 0.98 (bottom row), Ga = 1489 (e). The abscissa is normalized by the total energy injection rate ϵ^g. The dashed vertical line represents the wave number corresponding to bubble diameter, k_d. The continuous vertical line shows the wave number where the advective flux and the dissipative flux crosses. The region between these two lines, where the advective contribution dominates, is shaded with light blue color.

pseudo-turbulence regime for Ga ≤ 360 can be found in our earlier studies [14,15,22].

The scale-by-scale budget for high At = 0.8, 0.98.—We follow Refs. [28,30,31] to derive Eq. (3). We again consider statistical stationarity, hence $\partial_t \mathcal{E}_K = 0$. In Figs. 3(c) and 3(e), we plot all the terms of Eq. (3) as a function of K for both high and low Ga. The "baropycnal work," $\mathcal{P}_K$, now provide alternate routes for nonlinear energy transfer. The baropycnal term has contributions from the barotropic generation of strain and baroclinic generation of vorticity due to density variations [31]. Remarkably, for large enough Ga there is a range of scales, shaded in Figs. 3(c) and 3(e) where the dominant balance $\Pi_K \approx \epsilon^g/2$ is a constant leading to the Kolmogorov $-5/3$ scaling in the energy spectrum. The other transfer mechanisms $\mathcal{F}_K^\sigma$ and $\mathcal{P}_K$ are subdominant. A positive slope of $\mathcal{F}_K^\sigma$ ($\mathcal{P}_K$) indicates that the energy is absorbed (injected), whereas a negative slope indicates energy being injected (absorbed). Thus surface tension absorbs energy at large scales and injects it at small scales, whereas the opposite is the case for the baropycnal term.

Several earlier experimental and numerical studies [9–12,14–16,35,36] have shown that the power spectrum of velocity fluctuations is insensitive to variation in At for Ga ≲ 350. We have now shown that this is also true for large Ga. Thus, the following scenario emerges. For a fixed but small At, where the Boussinesq approximation is valid, the baropycnal flux is negligible. For a fixed but large At it is not. But even for the latter case as the Galilei number Ga is increased beyond some critical value Ga*, the advective flux can become the dominant contribution to the net flux. In such cases, Kolmogorov-like scaling holds. A systematic study to find out the how Ga* depends on At is outside the scope of this work.

We comment that the resolution required to conduct a fully resolved pseudo-turbulent simulation increases proportionally with both At and Ga [16,37]. However, a comparison of different experimental and numerical studies [11,14–16,36] reveals that the statistics of the velocity fluctuations, in particular, the PDF and the power spectra, are robust to the variation in both At and grid resolution. The effect of resolution is only observed at very small scales (see Supplemental Material [27], which includes Ref. [16]) and therefore we expect all our results will be valid at resolutions higher than the current study.

To conclude, we demonstrate, for the first time, that at large enough Ga > 1000, the power spectrum of velocity fluctuations shows the Kolmogorov scaling for range of scales between the bubble diameter and the dissipation scale. For scales smaller than η, the physics of pseudo-turbulence is recovered. Most of the earlier experiments on buoyancy driven bubbly flows have considered air bubbles of diameter $d \lesssim 5$ mm in water, which correspond to Ga ≲ 1000 [10,12]. Our study suggests that experiments with air bubbles of diameter $d \geq 7.5$ mm are needed to achieve Ga > 1000 and observe the Kolmogorov scaling range. At both high and low Atwood, we expect the $-5/3$ scaling range to increase further as the Ga is increased. Due to computational challenges [16], although such a study is currently not possible, it demands future investigations.

*vikash.pandey@su.se
†perlekar@tifrh.res.in

[1] G. Batchelor, *The Theory of Homogeneous Turbulence* (Cambridge University Press, Cambridge, England, 1953).

[2] J. Magnaudet and I. Eames, Annu. Rev. Fluid Mech. **32,** 659 (2000).

[3] R. F. Mudde, Annu. Rev. Fluid Mech. **37,** 393 (2005).

[4] S. L. Ceccio, Annu. Rev. Fluid Mech. **42,** 183 (2010).

[5] F. Risso, Annu. Rev. Fluid Mech. **50,** 25 (2018).

[6] E. Said, Annu. Rev. Fluid Mech. **51,** 217 (2019).

[7] V. Mathai, D. Lohse, and C. Sun, Annu. Rev. Fluid Mech. **11,** 529 (2020).

[8] M. Lance and J. Bataille, J. Fluid Mech. **222,** 95 (1991).

[9] J. M. Mercado, D. G. Gómez, D. V. Gils, C. Sun, and D. Lohse, J. Fluid Mech. **650,** 287 (2010).

[10] G. Riboux, F. Risso, and D. Legendre, J. Fluid Mech. **643,** 509 (2010).

[11] T. Ma, B. Ott, J. Fröhlich, and A. D. Bragg, J. Fluid Mech. **927,** A16 (2021).

[12] V. N. Prakash, J. M. Mercado, L. van Wijngaarden, E. Mancilla, Y. Tagawa, D. Lohse, and C. Sun, J. Fluid Mech. **791,** 174 (2016).

[13] E. Alméras, V. Mathai, D. Lohse, and C. Sun, J. Fluid Mech. **825,** 1091 (2017).

[14] V. Pandey, R. Ramadugu, and P. Perlekar, J. Fluid Mech. **884,** R6 (2020).

[15] V. Pandey, D. Mitra, and P. Perlekar, J. Fluid Mech. **932,** A19 (2022).

[16] A. Innocenti, A. Jaccod, S. Popinet, and S. Chibbaro, J. Fluid Mech. **918,** A23 (2021).

[17] U. Frisch, *Turbulence, A Legacy of A. N. Kolmogorov* (Cambridge University Press, Cambridge, England, 1997).

[18] S. Popinet, Annu. Rev. Fluid Mech. **50,** 49 (2018).

[19] G. Tryggvason, B. Bunner, A. Esmaeeli, D. Juric, N. Al-Rawahi, W. Tauber, J. Han, S. Nas, and Y.-J. Jan, J. Comput. Phys. **169,** 708 (2001).

[20] S. Chandrasekhar, *Hydrodynamic and Hydromagnetic Stability* (Dover Publications, New York, 1981).

[21] C. Canuto, M. Y. Hussaini, A. M. Quarteroni, and T. A. Zang, *Spectral Methods in Fluid Dynamics* (Springer-Verlag, Berlin, 2012).

[22] R. Ramadugu, V. Pandey, and P. Perlekar, Eur. Phys. J. E **43,** 73 (2020).

[23] S. Cox and P. Matthews, J. Comput. Phys. **176,** 430 (2002).

[24] W. Aniszewski, T. Arrufat, M. Crialesi-Esposito, S. Dabiri, D. Fuster, Y. Ling, J. Lu, L. Malan, S. Pal, R. Scardovelli, G. Tryggvason, P. Yecko, and S. Zaleski, Comput. Phys. Commun. **263,** 107849 (2021).

[25] A. Loisy, A. Naso, and P. D. M. Spelt, J. Fluid Mech. **816,** 94 (2017).

[26] In the Kolmogorov theory of single phase turbulence, the energy dissipation rate per unit mass is used. Since the problem at hand is multiphase flow, we use the injection rate per unit volume. They are simply related to each other by the factor of mean density ρ_a.

[27] See Supplemental Material at http://link.aps.org/supplemental/10.1103/PhysRevLett.131.114002 for detailed step-by-step derivation, which includes Refs. [17,28–31].

[28] S. Pope, *Turbulent Flows* (Cambridge University Press, Cambridge, England, 2012).

[29] G. Eyink, J. Stat. Phys. **78,** 335 (1995).

[30] H. Aluie, Physica (Amsterdam) **247D,** 54 (2013).

[31] A. Lees and H. Aluie, Fluids **92,** 1 (2019).

[32] L. Biferale and I. Procaccia, Phys. Rep. **414,** 43 (2005).

[33] M. K. Verma, *Energy Transfers in Fluid Flows* (Cambridge University Press, Cambridge, England, 2019).

[34] A. S. Monin and A. M. Yaglom, *Statistical Fluid Mechanics, Volume-2: Mechanics of Turbulence* (MIT, Cambridge MA, 1975).

[35] I. Roghair, J. M. Mercado, M. V. S. Annaland, H. Kuipers, C. Sun, and D. Lohse, Int. J. Multiphase Flow **37,** 1093 (2011).

[36] T. Ma, H. Hessenkemper, D. Lucas, and A. Bragg, J. Fluid Mech. **936,** A42 (2022).

[37] J. C. Cano-Lozano, C. Martinez-Bazan, J. Magnaudet, and J. Tchoufag, Phys. Rev. Fluids **1,** 053604 (2016).